LIMNOLOGY and OCEANOGRAPHY

ASLO

Limnol. Oceanogr. 68, 2023, 2108–2125

doi: 10.1002/lno.12409

High-frequency variability of carbon dioxide fluxes in tidal water over a temperate salt marsh

Shuzhen Song [1*] **Zhaohui Aleck Wang** [2*] **Kevin D. Kroeger** [3] **Meagan Eagle** [3] **Sophie N. Chu** [4] **Jianzhong Ge** [1]

[1]State Key Laboratory of Estuarine and Coastal Research, East China Normal University, Shanghai, China
[2]Department of Marine Chemistry and Geochemistry, Woods Hole Oceanographic Institution, Woods Hole, Massachusetts, USA
[3]U.S. Geological Survey, Woods Hole Coastal and Marine Science Center, Woods Hole, Massachusetts, USA
[4]Captura Corporation, Pasadena, California, USA

Abstract

Existing analyses of salt marsh carbon budgets rarely quantify carbon loss as CO_2 through the air–water interface in inundated marshes. This study estimates the variability of partial pressure of CO_2 (pCO_2) and air–water CO_2 fluxes over summer and fall of 2014 and 2015 using high-frequency measurements of tidal water pCO_2 in a salt marsh of the U.S. northeast region. Monthly mean CO_2 effluxes varied in the range of 5.4–25.6 mmol m^{-2} marsh d^{-1} (monthly median: 4.8–24.7 mmol m^{-2} marsh d^{-1}) during July to November from the tidal creek and tidally-inundated vegetated platform. The source of CO_2 effluxes was partitioned between the marsh and estuary using a mixing model. The monthly mean marsh-contributed CO_2 effluxes accounted for a dominant portion (69%) of total CO_2 effluxes in the inundated marsh, which was 3–23% (mean 13%) of the corresponding lateral flux rate of dissolved inorganic carbon (DIC) from marsh to estuary. Photosynthesis in tidal water substantially reduced the CO_2 evasion, accounting for 1–86% (mean 31%) of potential CO_2 evasion and 2–26% (mean 11%) of corresponding lateral transport DIC fluxes, indicating the important role of photosynthesis in controlling the air–water CO_2 evasion in the inundated salt marsh. This study demonstrates that CO_2 evasion from inundated salt marshes is a significant loss term for carbon that is fixed within marshes.

Salt marshes are among the most productive ecosystems and play a major role in the coastal carbon cycle (Cai 2011; Najjar et al. 2018). Net primary production in salt marshes is estimated to range from 150 to 1600 g C m^{-2} yr^{-1} (Duarte et al. 2005; Koeve and Oschlies 2012; Forbrich and Giblin 2015). A portion of carbon uptake by salt marshes (0–1700 g C m^{-2} yr^{-1}) is buried in sediments as "blue carbon" (McLeod et al. 2011; Hopkinson et al. 2012; Gonneea et al. 2019), thus helping to mitigate the increase of CO_2 in the atmosphere. The remaining fixed carbon leaves the marsh system via two interacting pathways. The first pathway is through lateral flux, driven by tidal water exchange between marshes and coastal waters. The export of dissolved inorganic carbon (DIC) and dissolved organic carbon (DOC) from salt marshes is an important source of carbon to estuarine and coastal waters (Osburn et al. 2015; Wang et al. 2016; Najjar et al. 2018). The second pathway for marsh carbon loss is through vertical evasion of respired CO_2 and methane (CH_4) via air–water exchange, plant-mediated transport, and marsh soil when exposed to the atmosphere (Cai et al. 2003; Chmura et al. 2011; Trifunovic et al. 2020).

CO_2 evasion from tidal water interactions with salt marshes is poorly constrained in the marsh carbon budget. When a salt marsh is inundated, marsh porewater exchanges with tidal water and adds large amounts of DIC and DOC to the water column that can be subsequently modified through physical and biogeochemical processes. These processes include water-column photosynthesis and respiration, air–water CO_2 exchange from inundated marsh platforms and tidal creeks, as well as lateral export of carbon from the marsh to the shelf

*Correspondence: zawang@whoi.edu and szsong@sklec.ecnu.edu.cn

Additional Supporting Information may be found in the online version of this article.

Author Contribution Statement: S.Z.S. led data analyses and the writing of the paper; she also obtained part of the fund to conduct this study. Z.A.W. co-led the paper; he conceptualized and conducted the main data analyses, wrote part of the paper and contributed to funding the study. K.D.K. assisted with data analysis and provided partial funding for the study. M.E. helped in collecting data and conducting data analysis. S.N.C. aided in data collection and analysis. J.Z.G. assisted in data analysis and modeling. All authors contributed to reviewing and editing the manuscript.

(Wang and Cai 2004; Dušek et al. 2009; Wang et al. 2016). The platform in this study refers to the vegetated portion of the marsh, distinct from tidal creeks or open water areas. Extremely high partial pressure of CO_2 (pCO_2) at low tides (> 10,000 μatm) in salt marsh tidal creeks (Wang and Cai 2004; Trifunovic et al. 2020; Chen et al. 2022) suggest that vertical CO_2 evasion across the air–water interface may be an important flux term for the marsh carbon budget. However, only a few studies have investigated and reported the air–water CO_2 flux in tidal creeks of salt marshes (Trifunovic et al. 2020; Chen et al. 2022). In addition to CO_2 flux from tidal creeks, CO_2 evasion is also expected to occur in the flooded marsh platform when water elevation is above the marsh. Wang and Cai (2004) first estimated the CO_2 efflux of an inundated marsh (including the tidal creek and flooded platform) using an approach that was coarse in spatiotemporal scales, where only high tide and low tide samples were collected in tidal creeks. In the preponderance of studies, respired CO_2 loss has been estimated using eddy covariance towers (e.g., Baldocchi 2014; Sanders-DeMott et al. 2022; Shahan et al. 2022) and static chamber methods (e.g., Kuehn et al. 2004; Moseman-Valtierra et al. 2016). These methods may have difficulty to specifically resolve vertical CO_2 fluxes via air–water exchange from other vertical CO_2 fluxes due to the relatively short duration and periodicities of tidal flooding on marsh platforms. Therefore, accurate quantification of the air–water CO_2 exchange occurring within marshes is warranted to gain insight on the significance of this flux pathway in wetland carbon budgets.

Furthermore, the proportion air–water CO_2 flux fueled by marsh carbon inputs to tidal creeks and inundated marsh platforms has not been clearly accounted for in the marsh carbon budget and lateral carbon exports. Previous CO_2 flux studies in salt marshes (e.g., Wang and Cai 2004; Trifunovic et al. 2020) rarely distinguish marsh-sourced CO_2 fluxes from estuarine-sourced or coast-sourced CO_2 fluxes as pCO_2 measurements in these studies measured bulk pCO_2 levels. This makes it difficult to account for the air–water CO_2 flux in the salt marsh carbon budget. To assess marsh carbon loss through air–water CO_2 exchange and to gain insight on the magnitude of this marsh carbon loss within the marsh carbon budget, it is important to separate the marsh carbon from estuarine carbon in the CO_2 flux. Moreover, tidal water CO_2 evasion could be affected by water-column photosynthesis and respiration. Photodegradation of DOC may also contribute to air–water CO_2 evasion, however, its contribution is likely small relative to respiration (Amaral et al. 2013; Vachon et al. 2016). Quantifying the magnitude of photosynthesis and respiration as a driver of air–water CO_2 flux would provide greater understanding of the internal carbon cycle in a salt marsh (Wang and Cai 2004; Cai 2011).

In this study, we present an analysis of high-frequency time-series measurements of pCO_2 and derived air–water CO_2 effluxes over daily to seasonal time scales, in a northeast U.S. temperate salt marsh. CO_2 effluxes were estimated from the water surface, both in the tidal creek, and in the tidally-flooded marsh platform. The total CO_2 evasion and vertical loss of marsh carbon through the air–water interface were quantified by distinguishing the marsh-sourced carbon evasion from the estuarine-sourced carbon evasion in the inundated area. The influence of photosynthesis on this evasion was also quantified. Finally, the marsh-sourced CO_2 evasion flux from inundated marshes was integrated into the marsh carbon budget along the U.S. northeastern coast to gain a better understanding of the major loss terms in the marsh carbon cycle. To the best of our knowledge, this study is the first to distinguish between marsh and estuarine provenance for evaded CO_2 from a tidal creek and inundated platform with high-frequency measurements.

Methods

Study site

The study site, Sage Lot Pond (SLP), is an intertidal salt marsh located near the eastern inlet of Waquoit Bay, on Cape Cod, Massachusetts (Fig. 1). There is no river input near the marsh, and groundwater is a small source of freshwater in the study area, only accounting for 3% of the mean annual tidal flow (Wang et al. 2016; Chu et al. 2018). The vegetation community is dominated by *Spartina alterniflora* in low marsh areas, and *Distichlis spicata* and *Juncus gerardii* in high marsh areas.

The time-series sampling site was located at the mouth of a tidal creek (Fig. 1b). The water depth in the tidal creek ranged from 0.2 to 1.1 m with the maximum observed in autumn (Chu et al. 2018). The drainage area (4132 m^2) was defined using a water routing analysis with a 1-m bare-earth LiDAR-derived digital elevation model (DEM) (Wang et al. 2016). This drainage area, coupled with a hydrodynamic model and water flow data, has been used to determine area-normalized DIC fluxes from the SLP salt marsh (Wang et al. 2016).

Measurements

In situ high-frequency measurements of surface water elevation (m), salinity, temperature (°C), and dissolved oxygen (DO; mg L^{-1}) were conducted from August 2014 to November 2015 using an EXO2 Multiparameter Sonde (YSI Inc.) deployed at ~ 0.2 m below the water surface in a tidal creek with data interpolated to 5 min. Water elevation was measured by a SonTek IQ Plus acoustic Doppler velocity meter (Sontek/YSI) located 3 m upstream of the EXO2 every 5 min. The relative elevation of the deployed Sontek IQ Plus was referenced to NAVD88. All sensors were calibrated according to recommended methods of the manufacturer before and after the measurements. Photosynthetic active radiation (PAR; mmol m^{-2} s^{-1}) data was collected at the site from 2014 to 2015 (Data accessed from the Waquoit Bay National Estuarine Research Reserve website: http://waquoitbayreserve.org/

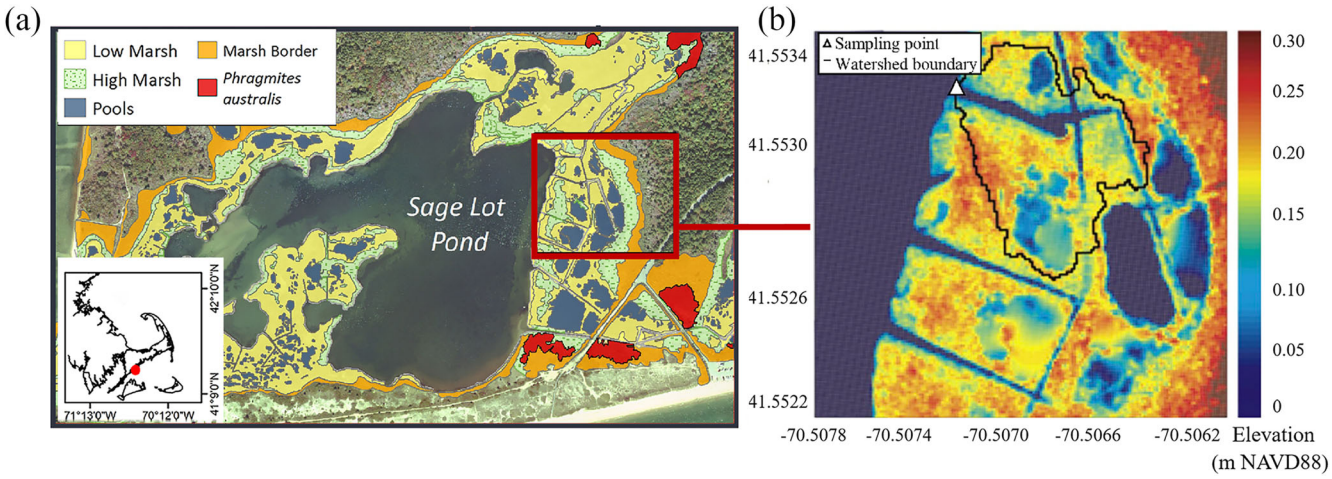

Fig. 1. Study site. (**a**) The salt marsh habitat map of Sage Lot Pond and its location in the Waquoit Bay, Massachusetts, USA; (**b**) the location of the time-series sampling site, with the corresponding drainage area (black line) and water elevation (color).

research-monitoring/biomonitoring-salt-marsh-sav/; accessed 09 October 2021). Wind speed measured at 3 m height was recorded in 10-min intervals (Data accessed from the NOAA National Estuarine Research Reserve System Centralized Data Management Office website: http://www.nerrsdata.org; accessed 03 July 2021). The wind speed was transformed to corresponding values at 10 m above sea surface according to Large and Pond (1981). Atmospheric pCO_2 time-series are from Mooring_NH_70W_43N in the North Atlantic Ocean, $\sim$ 170 km away from the study site, downloaded from NOAA National Centers for Environmental Information at: https://doi.org/10.3334/cdiac/otg.tsm_papa_145w_50n; accessed 10 November 2021.

A high-frequency Mini CO_2 sensor (Pro-Oceanus Systems Inc.) was deployed adjacent to the EXO2 to measure pCO_2 in the tidal water surface (41.5533°N, −70.5072°W; Fig. 1b) for time periods from 2013 to 2016. The sensor has a semipermeable membrane to allow rapid diffusion of dissolved CO_2 from the surrounding water into a gas headspace, where a non-dispersive infrared detector measures CO_2. The pCO_2 measurements were corrected for pressure effect and recorded at 2-s frequency in continuous mode. The sensor was calibrated by Pro-Oceanus prior to deployment, and checked monthly to change the battery and clean the instrument during deployment. In this study, we used the data collected in 2014 and 2015 for the high-resolution pCO_2 data analysis since data coverage during 2013 and 2016 was too sparse to include. To assess the quality of pCO_2 sensor data, we compared the sensor data with pCO_2 calculated from the bottle-measured DIC-potentiometric pH pair or DIC-spectrophotometric pH pair. The potentiometric pH was measured with a ROSS combination electrode (Thermo Fisher Scientific) at 22.4 ± 0.1°C with a precision of $\sim$ 0.02. The electrode was calibrated using three National Bureau of Standards solutions (pH 4.01, 7.00, and 10.01). The spectrophotometric pH was measured with a UV–visible spectrophotometer (Agilent 8454; Agilent Technologies) using purified meta-cresol purple as an indicator (Douglas and Byrne 2017). The uncertainty of the spectrophotometric pH measurement was ± 0.006 on the total proton concentration scale. The DIC samples were measured by a DIC auto-analyzer (AS-C3; Apollo SciTech Inc.) with a precision of ± 2 μmol kg^{-1} (Data accessed from the Biological and Chemical Oceanography Data Management Office [BCO-DMO] website: https://www.bco-dmo.org/dataset/794163; accessed 06 November 2021). Due to time elapsed while collecting water samples, discrete samples were likely integrated over several minutes, so pCO_2 sensor data were binned over a 10-min interval to match the bottle samples. The binned pCO_2 sensor data were compared to the corresponding calculated pCO_2 data from the DIC-potentiometric pH or the DIC-spectrophotometric pH pair through a CO_2 system parameter calculation program (CO2SYS v3; Sharp et al. 2020) in 2013, 2015, and 2016 (calculated pCO_2 data were not available in 2014) (Supporting Information Fig. S1). For pCO_2 calculation, dissociation constants of carbonic acid, boric acid, and hydrogen fluoride were taken from Cai and Wang (1998), Dickson (1990), and Dickson and Riley (1979), respectively. There is a good agreement between the sensor data and calculated pCO_2 values derived from both potentiometric pH ($R^2 = 0.867$ in 2013, $n = 13$; $R^2 = 0.908$ in 2015, $n = 37$; $R^2 = 0.883$ in 2016, $n = 28$) and spectrophotometric pH ($R^2 = 0.864$ in 2016, $n = 28$). The discrepancies partially resulted from the uncertainties of pCO_2 calculations and measurement uncertainties of discrete DIC and pH samples. Potentiometric pH measurements may bear large uncertainties (> 0.01; Dickson et al. 2007). The spectrophotometric pH measurement could be potentially influenced by colored dissolved organic matter, though the impact could be small as all samples were measured as "blanks" before pH indicator addition, which should correct original water color in samples (Song et al. 2020).

Overall, the Mini CO_2 sensor provided high-resolution pCO_2 measurements with reasonably good quality that is suitable for the analysis conducted in this paper.

Machine learning algorithm for pCO_2

To fill pCO_2 data gaps during the sampling periods when the sensor was not deployed, we applied the feed-forward network (FFN) method, a deep learning algorithm, to model tidal water pCO_2 at the time-series SLP site using time of the year, temperature, salinity, DO, and water elevation as the input variables. The FFN method has been applied to fill data gaps of ocean surface pCO_2 observations (Rödenbeck et al. 2013; Landschützer et al. 2014). The datasets were normalized according to the mean and standard deviation of each variable (except time of the year) before training by the algorithm. About 80% of the datasets were used in algorithm training and the rest ~ 20% were used for algorithm validation. The coefficient of determination (r^2) was 95% over the sampling period in 2014 and 2015. The root-mean-squared errors were 156 μatm in 2014 and 124 μatm in 2015, respectively.

Statistical analysis of pCO_2 controlling factors

A principal component analysis (PCA) was applied using IBM SPSS Statistics 23 (IBM Corp.) to determine the major factors influencing pCO_2 variability in summer and fall, similar to previous examinations of the variability in seawater pCO_2 and CO_2 flux (Lohrenz et al. 2010; Abdul-Aziz et al. 2018). PCA analysis was conducted only with the sensor-measured pCO_2 data (indicated in Fig. 3) associated with salinity, temperature, water elevation, DO, and PAR datasets. FFN modeled pCO_2 data were not used for this analysis.

Air–water CO_2 flux

The hourly total CO_2 fluxes across the air–water interface at the mouth of the tidal creek ($tFCO_{2\text{-creek}}$; mmol m^{-2} water h^{-1}) were calculated as:

$$tFCO_{2-\text{creek}} = k\beta(pCO_{2w} - pCO_{2a}), \quad (1)$$

where k (cm h^{-1}) is the gas transfer velocity; β is the solubility of CO_2 (mol L^{-1} atm^{-1}; Weiss 1974); pCO_{2w} and pCO_{2a} are pCO_2 measured in the surface water and atmosphere, respectively. The k values were calculated using the empirical equation of wind speed developed for shallow and microtidal estuaries by van Dam et al. (2019) (hereafter referred to as the D method; Eq. 2):

$$k\left(\text{cm h}^{-1}\right) = (4.2 + 1.5\mu)(Sc/600)^{-0.5}, \quad (2)$$

μ (m s^{-1})- is the average wind speed at a height of 10 m. Sc is the Schmidt number for CO_2 at a given temperature and salinity. The D method provided a moderate k value (Supporting Information Table S1), compared to the k values based on equations from Raymond and Cole (2001) and Borges et al. (2004), which have been used in estuaries and tidal creeks (e.g., Atkins et al. 2013; Call et al. 2015; Santos et al. 2019). Moreover, van Dam et al. (2019) found the relationship between gas transfer velocity and wind speed during daytime was different from that at nighttime, likely due to the difference of water-side thermal convection between nighttime and daytime. Currently, there is no consensus on the k value parameterization in estuarine and shallow coastal systems (Borges et al. 2004; Ho et al. 2018). We chose the D method over others for calculation of k is because their measurement conditions are mostly relevant to ours. We applied the D method to estimate the hourly air–water CO_2 flux, and quantify the factors influencing its day–night variability.

The time-varying inundated marsh platform area within the study domain was determined based on output from an implementation of the COAWST hydrodynamic model (Warner et al. 2010; Wang et al. 2016) and supported by a 1-m bare-earth LiDAR DEM (NAVD88), with continuous data on water levels and flow at the creek mouth. Comparison of LiDAR elevation data with RTK GPS elevation indicated minimal bias and error. To estimate the total air–water CO_2 flux across the inundated area, including the tidal creek and marsh platform, we assumed the pCO_2 value at the mouth of the tidal creek was representative of the water flooding the platform. The total CO_2 evasion rate over the inundated marsh was then calculated by multiplying $tFCO_{2\text{-creek}}$ (mmol m^{-2} water h^{-1}) by the time-varying area of inundated marsh ($A_{\text{-inmarsh}}$; m^2) at a given tide stage, including the inundated marsh platform and the tidal creek area. The total area-normalized CO_2 evasion fluxes in the marsh drainage area ($tFCO_{2\text{-inmarsh}}$; mmol m^{-2} marsh h^{-1}) were then calculated using the marsh drainage area of $A = 4132$ m^2:

$$tFCO_{2-\text{inmarsh}} = tFCO_{2-\text{creek}} \times A_{-\text{inmarsh}}/A. \quad (3)$$

A positive value indicates the inundated marsh is a source of atmospheric CO_2, while a negative value means that the inundated marsh is a CO_2 sink. In this study, we report the area-normalized $tFCO_{2\text{-inmarsh}}$ value of the marsh drainage area in order to compare with other marsh area normalized carbon fluxes (e.g., lateral DIC and DOC export fluxes).

Marsh-contributed CO_2 flux

It is important to quantify marsh carbon loss as CO_2 from tidal water as it is likely an important term in the marsh carbon cycle. pCO_2 in tidal water flooding the marsh was influenced by mixing between estuarine water, marsh porewater, and groundwater, and biogeochemical processes (e.g., photosynthesis and respiration) in the water. As the fresh and brackish groundwater only contributed to a small proportion (~ 8.6%) of DIC in the study area (Wang et al. 2016; Tamborski et al. 2021), pCO_2 and the corresponding CO_2 flux contributed by groundwater was likely insignificant. The increase of pCO_2 over high–low tidal cycles is thus primarily sourced from marsh porewater and from

the net effect of water-column respiration and photosynthesis within the marsh study domain. We define this pCO_2 increase as marsh-sourced pCO_2 ($(pCO_2)_m$), which mostly derives from respirations in marsh porewater and less in tidal water (Zhu et al. 2022). The air–water CO_2 flux derived from marsh-sourced pCO_2 was defined as marsh-contributed CO_2 flux. Similarly, the air–water CO_2 flux contributed by estuarine-sourced pCO_2 was defined as estuarine-contributed CO_2 flux. At a given time or in a short-time period (minutes), the CO_2 flux at the mouth of the tidal creek is almost proportional to pCO_2, since the other terms in the flux calculation do not change significantly (Eq. 1). We can thus assume that the marsh-contributed CO_2 flux is proportional to marsh-sourced pCO_2 at a given moment. This leads to the ratio of marsh-contributed CO_2 flux to total CO_2 flux at the mouth of the tidal creek ($R_{(FCO2)m}$) being approximately equal to the ratio of marsh-sourced pCO_2 to measured pCO_2 in the tidal water ($R_{(pCO2)m}$). The hourly marsh-contributed CO_2 flux at the mouth of tidal creek ($(FCO_{2\text{-creek}})_{mc}$; mmol m^{-2} water h^{-1}) can then be calculated by multiplying the hourly total CO_2 flux (i.e., $tFCO_{2\text{-creek}}$; mmol m^{-2} water h^{-1}) by $R_{(pCO2)m}$:

$$(FCO_{2-creek})_{mc} = R_{(FCO2)m} \times tFCO_{2-creek} = R_{(pCO2)m} \times tFCO_{2-creek} \quad (4)$$

We defined the peak high tide during each 24-h period as the estuarine endmember. We assumed that the [CO_2*] concentration in the estuarine endmember remained constant over each daily period. For instance, in the absence of substantial external inputs, previous reports have indicated only small variations (< 6 μmol kg^{-1}) in [CO_2*] in the nearshore water of the Gulf of Maine (~ 160 km north from the study site) in summer and autumn (Data accessed from the NOAA National Centers for Environmental Information website: https://doi.org/10.3334/cdiac/otg.tsm_unh_gom; accessed 01 October 2021). Moreover, since pCO_2 values vary with temperature and salinity in addition to other physical and biogeochemical processes, we used [CO_2*], which is conservative relative to salinity and temperature variations, as a constant value in the estuarine endmember over each daily time scale. The estuarine-sourced pCO_2 ($(pCO_2)_e$) at a given time was then calculated from [CO_2*] at the peak high tide (the estuarine endmember) using the corresponding salinity and temperature at that time according to the CO_2 solubility equation (Weiss 1974). Therefore, the ratio (i.e., $R_{(pCO2)m}$) of marsh-sourced pCO_2 to observed pCO_2 in the tidal water at a given time was calculated as:

$$R_{(pCO2)m} = \frac{pCO_2 - (pCO_2)_e}{pCO_2}. \quad (5)$$

The hourly marsh-contributed CO_2 flux at the mouth of tidal creek was then derived according to Eqs. 4, 5. Similarly, the net marsh-contributed CO_2 flux in inundated marsh (i.e., $(FCO_{2\text{-inmarsh}})_{mc}$; mmol m^{-2} marsh h^{-1}) was derived by multiplying hourly marsh-contributed CO_2 flux at the mouth of tidal creek (mmol m^{-2} water h^{-1}) by the corresponding inundated area and then normalizing to the marsh drainage area:

$$(FCO_{2-inmarsh})_{mc} = (FCO_{2-creek})_{mc} \times A_{-inmarsh}/A. \quad (6)$$

The hourly marsh-contributed CO_2 flux at the mouth of tidal creek and in inundated marsh were then integrated into a whole day to derive the corresponding daily flux.

Photosynthetic impact on CO_2 flux

During the daytime, water-column CO_2 may be influenced by photosynthesis, resulting in reduction of CO_2 evasion in tidal water. The CO_2 flux reduction due to photosynthesis was defined as the photosynthetic impact on CO_2 flux in this study. Noting that the reduction in CO_2 flux due to photosynthesis does not equal the in-water photosynthetic rate, given that the total DIC ($HCO_3^- + CO_3^{2-} + [CO_2*]$), not just [$CO_2$*], can be assimilated by photosynthesis. In addition to photosynthesis, CO_2 in the tidal water may be primarily influenced by respiration in the water column, and mixing between estuarine water and marsh porewater in which CO_2 is essentially derived from respiration of estuarine and marsh soil carbon. Herein, we define the CO_2 derived from these physical and biogeochemical processes other than photosynthesis as respiration-derived CO_2. Given likely insignificant contribution of photochemical degradation of organic carbon to CO_2 relative to biological respiration in tidal water (Amaral et al. 2013; Vachon et al. 2016), we assume their effect on CO_2 evasion was negligible. Therefore, the daily total CO_2 flux, $tFCO_{2\text{-creek}}$, at the mouth of the tidal creek (mmol m^{-2} water d^{-1}) was treated as the sum of photosynthetic impact on CO_2 flux ($(FCO_{2\text{-creek}})_P$; mmol m^{-2} water d^{-1}) and daily respiration-derived CO_2 flux ($(FCO_{2\text{-creek}})_R$; mmol m^{-2} water d^{-1}):

$$tFCO_{2-creek} = (FCO_{2-creek})_P + (FCO_{2-creek})_R \quad (7)$$

In this study, we defined the nighttime when PAR = 0. At nighttime, the respiration-derived CO_2 flux at the mouth of the tidal creek provides a measure of air–water CO_2 flux in the absence of photosynthesis. To quantify the photosynthetic impact on CO_2 flux, we assumed that the average respiration-derived CO_2 concentration was equivalent at day and night. Furthermore, if the gas transfer velocity (largely controlled by wind speed) was equivalent between day and night, the average respiration-derived creek CO_2 fluxes would also be the same over a day. However, large differences in wind speed between daytime and nighttime (up to 5 m/s) were observed. To account for this difference, the average hourly daytime respiration-derived creek CO_2 fluxes were scaled from the corresponding average hourly nighttime CO_2 flux by using the ratio of the day–night gas transfer velocities, and then integrated into the daytime respiration-derived creek CO_2 fluxes by multiplying daytime hours. The daily respiration-

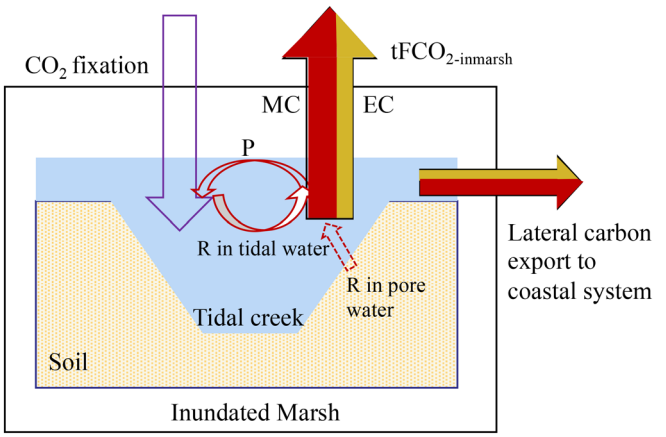

Fig. 2. A schematic of air–water CO_2 and carbon fluxes in an inundated marsh discussed in this study. $tFCO_{2\text{-inmarsh}}$ represents the total CO_2 fluxes in the inundated marsh. MC and EC represent the marsh-contributed ($(FCO_{2\text{-inmarsh}})_{MC}$; red color shade in the $tFCO_{2\text{-inmarsh}}$ arrow) and estuarine-contributed CO_2 fluxes ($(FCO_{2\text{-inmarsh}})_{EC}$; orange color shade in the $tFCO_{2\text{-inmarsh}}$ arrow) in the inundated marsh, respectively. P denotes the impact of photosynthesis on CO_2 flux in the inundated marsh, that is, the amount of CO_2 flux reduced by photosynthesis ($(FCO_{2\text{-inmarsh}})_P$). R represents the contribution of respiration in tidal water or marsh porewater to air–water CO_2 flux.

derived creek CO_2 flux (i.e., $(FCO_{2\text{-creek}})_R$) was the sum of the nighttime CO_2 flux and the daytime respiration-derived creek CO_2 flux, which was used to derive the photosynthetic impact on CO_2 flux at the mouth of tidal creek according to Eq. 7.

In the inundated marsh, the daily respiration-derived CO_2 flux ($(FCO_{2\text{-inmarsh}})_R$; mmol m^{-2} marsh d^{-1}) and photosynthetic impact on CO_2 flux ($(FCO_{2\text{-inmarsh}})_P$; mmol m^{-2} marsh d^{-1}) were calculated by normalizing creek flux values to the marsh drainage area similar to Eq. 6:

$$(FCO_{2-\text{inmarsh}})_R = (FCO_{2-\text{creek}})_R \times A_{-\text{inmarsh}}/A, \quad (8)$$

$$(FCO_{2-\text{inmarsh}})_P = (FCO_{2-\text{creek}})_P \times A_{-\text{inmarsh}}/A. \quad (9)$$

A negative value for photosynthetic impact on CO_2 flux indicates CO_2 in the tidal water was assimilated by photosynthesis while the marsh was flooded.

Fig. 2 shows the defined CO_2 and carbon fluxes in an inundated marsh to facilitate understanding of the analysis reported in this study.

Results

Temporal variations in pCO_2

The deep learning algorithm predicted pCO_2 shows good agreement with the sensor-measured pCO_2 (Fig. 3). Due to the missing measurements of temperature, salinity or water elevation, the pCO_2 data gaps over some time periods were not filled by the algorithm (Fig. 3; Supporting Information Fig. S2). The mean daily pCO_2 values generally decreased from summer to late fall (Fig. 3) as a result of lower respiration and cooler weather.

We assessed tidal variations in pCO_2, water elevation, salinity, temperature, PAR, and DO over 11-d period covering spring and neap tides in August 2014 (Fig. 4), to demonstrate tidal variations in pCO_2 and other environmental parameters. Superimposed on the day–night cycle, nighttime DO concentrations generally decreased from high tide to low tide, indicating lower DO concentrations of tidal water after exchange with the marsh (Fig. 4). pCO_2 was generally negatively

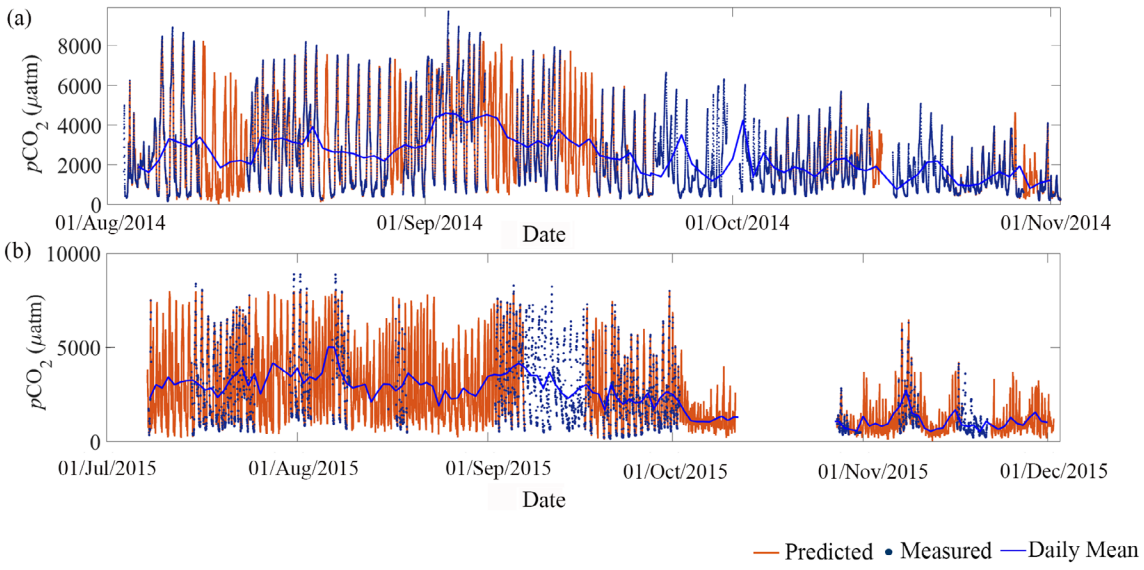

Fig. 3. Measured pCO_2 (blue circles) and predicted pCO_2 (orange lines) using deep learning algorithms with daily mean pCO_2 values (blue lines) for the sampling periods of 2014 (a) and 2015 (b).

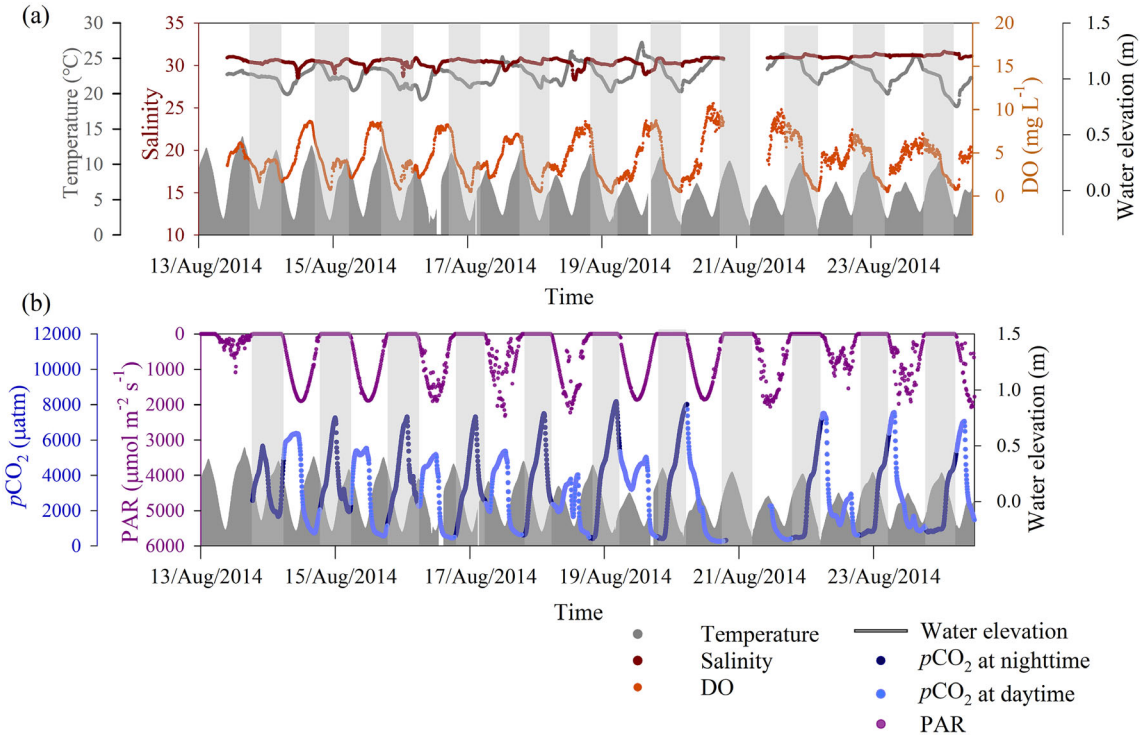

Fig. 4. Variations in water elevation, salinity, temperature, DO (**a**), PAR, and pCO_2 (**b**) in August 2014. Shaded regions indicate nighttime.

correlated with water elevation with the maximum pCO_2 over each day observed at the peak low tide, and increased as water elevation decreased, especially at nighttime (Fig. 4). This suggests the export of DIC from the marsh may play a significant role in driving tidal water pCO_2. This observation is consistent with the previous studies at SLP (Wang et al. 2016; Chu et al. 2018).

Factors driving pCO_2 variability

PCA was conducted to gain insight into the potential environmental factors influencing variations in tidal water pCO_2 over summer and autumn (Fig. 5). Two principal components accounted for 68.3% in summer and 70.3% in autumn of total variance for pCO_2, DO, water elevation, temperature (T), salinity, cumulative PAR, and pH over two years (Fig. 5). The cumulative PAR value at a specific daytime point was determined by summing up PAR values from the beginning of daytime until that particular time point, whereas cumulative PAR was considered to be zero at nighttime. Cumulative PAR was employed to align with pCO_2, which reflects a cumulative response to multiple drivers, including biological (e.g., respiration and photosynthesis) and physical processes (e.g., mixing), on a range of timescales. The correlation rank for all variables is shown in Supporting Information Table S2, S3.

In summer, pCO_2 had a negative loading on the first principal component (PC1), while T, pH, DO, and cumulative PAR had positive loadings with high values (Fig. 5a). Given primary production can be positively correlated with T, cumulative PAR, pH, and DO values but negatively correlated with pCO_2 values (Nezlin et al. 2009; Raven et al. 2020), we suspect PC1 represents the primary production in this study. For the second principal component (PC2), pCO_2 still had a negative loading, while water elevation had a positive loading with a high absolute value (Fig. 5a). We thus presume PC2 represents the mixing between tidal water and marsh porewater. Therefore, primary production and the mixing between tidal water and marsh porewater were likely two important factors influencing variations in tidal water pCO_2. Given the higher absolute loading of pCO_2 on PC1 than PC2 (Fig. 5a), we suggest primary production might be a principal factor influencing variations in tidal water pCO_2 in the summer.

In autumn, water elevation, pH, and DO had high and positive loadings on PC1, while pCO_2 had a significantly negative loading (Fig. 5b). Given that the tidal flooding increased water elevation, pH, and DO values and decreased pCO_2 values in tidal water, we suggest that here PC1 might represent the influence of tidal water flooding and mixing. PC2 might represent the factors correlated with temperature, given the high loading of temperature on PC2 (Fig. 5b). The magnitude of pCO_2 loading on PC1 was much greater than PC2 (Fig. 5b), so we suggest mixing between tidal water and marsh porewater was a primary factor influencing tidal water pCO_2 in autumn. The low tide samples were much closer to the direction of pCO_2 arrow in both summer and autumn, while high tide

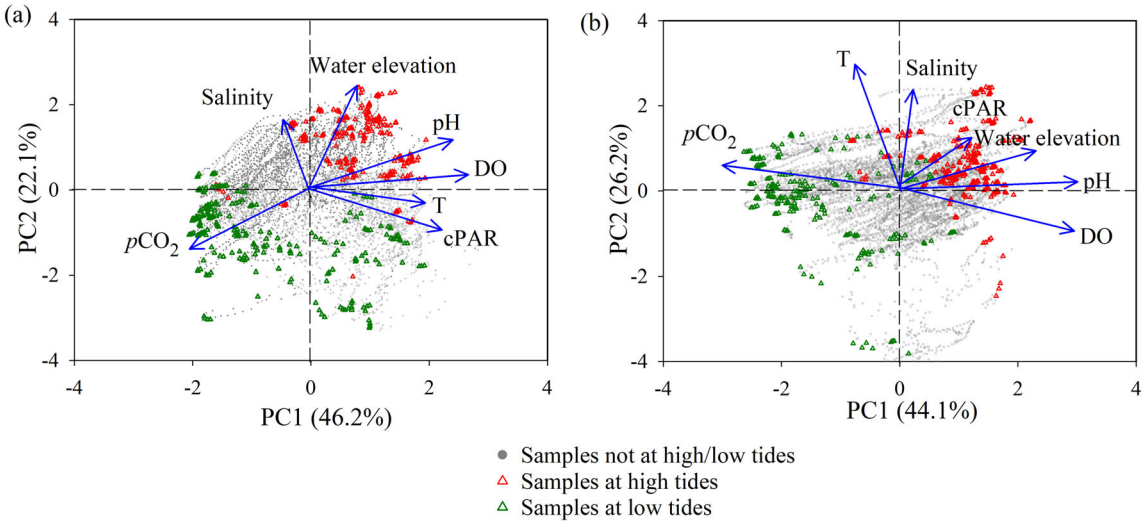

Fig. 5. The PCA correlation biplot of variables including pCO_2, cumulative PAR (cPAR), water elevation, temperature (*T*), pH, DO, and salinity in summer (**a**) and autumn (**b**) of 2014 and 2015. The data points in the plot indicate the scores of each sample projected onto the principal components. The length and direction of the arrows indicate the strength and direction of the relationship between the variables and the principal components. Samples at high/low tides refer to the samples collected within a 1-h window around the water elevation reached the maximum or minimum values within each tidal cycle.

samples were more distant, indicating a high level of pCO_2 at low tides (Fig. 5). This is consistent with the previous finding that marsh porewater contributes a considerable amount to pCO_2 in tidal water exchanged with the salt marsh (Wang et al. 2016; Tamborski et al. 2021).

Temporal variations in CO_2 flux

Daily CO_2 fluxes at the mouth of the SLP tidal creek (i.e., $tFCO_{2\text{-creek}}$) and CO_2 fluxes from the inundated marsh (i.e., $tFCO_{2\text{-inmarsh}}$) including the tidal creek and inundated marsh platform were highly variable over the study period in 2014, as were daily mean pCO_2, wind speed, and inundated area (Fig. 6). The daily inundated marsh CO_2 flux was positively and significantly correlated with pCO_2, wind speed, water elevation, and inundated marsh area (Supporting Information Table S4), indicating the importance of these variables in affecting air–water CO_2 fluxes in the inundated marsh. The weekly mean CO_2 fluxes were only shown when all daily values over this time period were available. The monthly mean/median creek and inundated marsh CO_2 fluxes were calculated from daily CO_2 fluxes with linear interpolation of missing values. All relevant monthly mean/median CO_2 fluxes presented below were calculated this way. Both the maximum weekly mean and monthly mean/median of CO_2 fluxes from inundated marsh in 2014 were observed in September, likely resulting from high daily and weekly mean pCO_2 values over this period (Fig. 6).

The maximum daily creek CO_2 flux in 2015 occurred in July, while the maximum inundated marsh CO_2 flux was observed in September, coincident with greater inundated area and high pCO_2 value in September (Fig. 7a,b). The monthly mean/median CO_2 flux from inundated marsh showed a decreasing trend from July to November 2015, however, the maximum weekly mean inundated marsh CO_2 flux was observed in September (Fig. 7).

Marsh-contributed CO_2 flux

To gain insights on the proportion of marsh vs. estuarine contributions to the air–water CO_2 efflux from tidal water, the daily and weekly mean of estuarine-contributed CO_2 flux ($(FCO_{2\text{-inmarsh}})_{ec}$) and marsh-contributed CO_2 flux ($(FCO_{2\text{-inmarsh}})_{mc}$) from the inundated marsh were compared over the sampled months in 2014 and 2015 (Fig. 8). The marsh-contributed CO_2 flux was calculated at nighttime and daytime separately in order to show the strong day–night variability and the influence by photosynthesis and respiration over tidal cycles (Fig. 8). In contrast to nighttime marsh-contributed CO_2 fluxes, more marsh carbon evaded at daytime during summer and early autumn (Fig. 8). The daily mean marsh contribution accounted for 17–98% (mean = ~ 69%) of the total CO_2 effluxes in 2014 and 2015, with the remaining ~ 31% on average sourced from estuarine carbon (Fig. 8). Marsh-sourced carbon thus predominantly contributed to the air–water CO_2 efflux from the inundated marsh. Both the daily mean marsh-contributed CO_2 flux and estuarine-contributed CO_2 flux were significantly correlated ($p < 0.01$) with the water elevation and total CO_2 efflux from the inundated marsh over the study periods of 2014 and 2015 (Supporting Information Table S4). Nevertheless, higher water elevation increased estuarine water flooding, coincident with a greater proportion of estuarine-sourced CO_2 in tidal water exchanged with the salt marsh, leading to relatively high percentages of estuarine-contributed CO_2 fluxes and low percentages of marsh-contributed CO_2 fluxes to the total CO_2 effluxes from

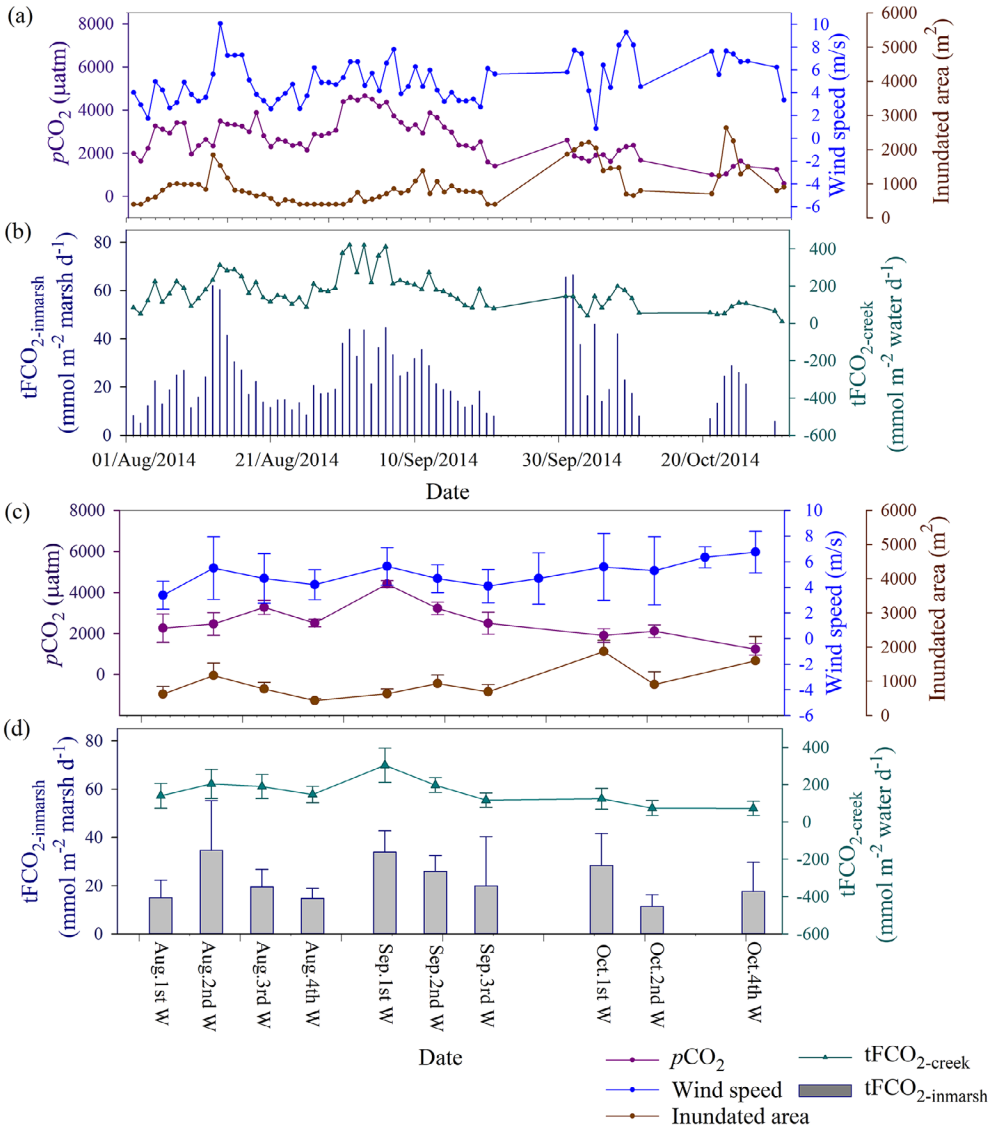

$tFCO_{2\text{-inmarsh}}$ (mmol m^{-2} marsh d^{-1})	August	September	October
Monthly mean/median	21.5/17.4	25.5/24.6	25.4/21.2

Fig. 6. Daily (**a**, **b**) and weekly (**c**, **d**) mean pCO_2, inundated area, wind speed, and total CO_2 effluxes at the mouth of the SLP tidal creek ($tFCO_{2\text{-creek}}$) and in the inundated marsh ($tFCO_{2\text{-inmarsh}}$) in 2014. The table below the figure shows the monthly means and medians of CO_2 effluxes in the inundated marsh ($tFCO_{2\text{-inmarsh}}$). W in the *x*-axis label (**d**) means week.

inundated marsh over some studied periods, especially in October 2014 (Fig. 8; Supporting Information Fig. S2).

The weekly mean of marsh-contributed CO_2 flux was highly variable over the studied months in both years, especially in 2014 (Fig. 8b,d). In 2014, the maximum monthly mean/median of the marsh-contributed CO_2 flux was observed in September (Fig. 8). In comparison, this flux value decreased from July to November in 2015 with its proportion in total CO_2 effluxes reaching a maximum in September (Fig. 8). The monthly mean/median of marsh-contributed CO_2 flux was higher in August 2015 than in August 2014, but lower in September 2015 than in September 2014 (Fig. 8).

Impact of photosynthesis on CO_2 flux

The daily impact of photosynthesis on CO_2 fluxes, $(FCO_{2\text{-inmarsh}})_P$, was assessed by comparing these flux values to the daily respiration-derived CO_2 effluxes $(FCO_{2\text{-inmarsh}})_R$, in the inundated marsh over the sampled months in 2014 and 2015 (Fig. 9). In 2014, the daily photosynthetic impact on CO_2 fluxes varied from −1 to −72 mmol m^{-2} marsh d^{-1} from

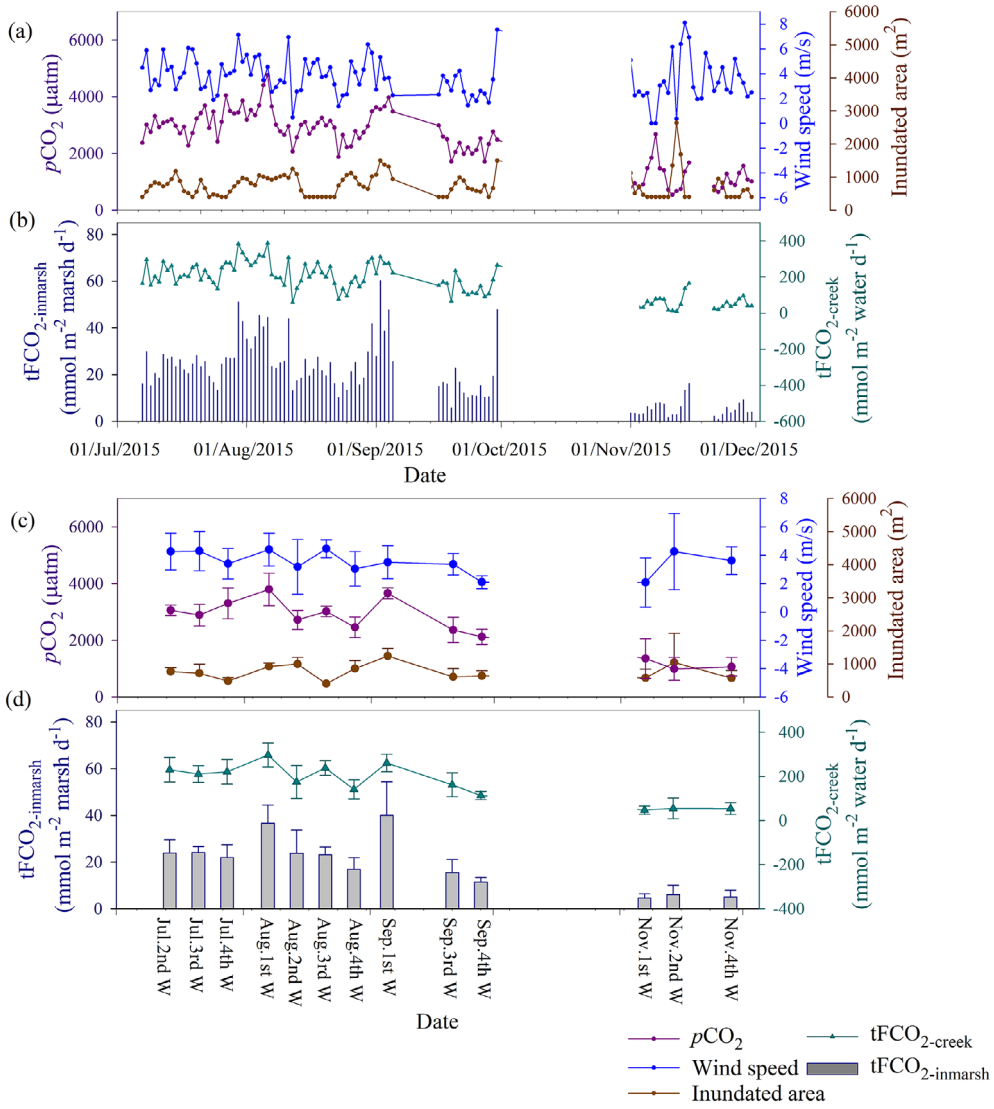

$tFCO_{2\text{-inmarsh}}$ (mmol m^{-2} marsh d^{-1})	July	August	September	November
Monthly mean/median	25.0/24.7	25.6/21.8	22.0/16.8	5.4/4.8

Fig. 7. Daily (**a**, **b**) and weekly (**c**, **d**) mean pCO_2, inundated area, wind speed, and total CO_2 effluxes at the mouth of the SLP tidal creek ($tFCO_{2\text{-creek}}$) and in the inundated marsh ($tFCO_{2\text{-inmarsh}}$) in 2015. The table below the figure shows the monthly means and medians of CO_2 effluxes in the inundated marsh ($tFCO_{2\text{-inmarsh}}$). W in the *x*-axis label (**d**) means week.

August to October (Fig. 9a). This translates to a reduction in respiration-derived CO_2 effluxes by 4–69% (mean 33%; Fig. 9a), which equaled 4–223% (mean 64%) of the corresponding total CO_2 effluxes from the inundated marsh. Such a reduction reached a maximum in August (Fig. 9a). In 2015, the photosynthetic impact on CO_2 fluxes varied from −1 to −56 mmol m^{-2} marsh d^{-1} with the minimum observed at the end of September, effectively reducing respiration-derived CO_2 effluxes by 1–86% (mean 30%; Fig. 9c). These reduced fluxes equaled 1–307% (mean 58%) of the corresponding total CO_2 effluxes. The photosynthetic impact on CO_2 flux was negatively and significantly correlated with the total CO_2 efflux from inundated marsh, and marsh-contributed CO_2 flux (Supporting Information Table S4), likely resulting from similar seasonal variations between carbon assimilation rate and respiration rate.

The weekly mean and monthly mean/median respiration-derived CO_2 effluxes and photosynthetic impact on CO_2 fluxes in the inundated marsh were also highly variable over the study periods of both years (Fig. 9). In 2014, both the absolute maximum values of weekly mean and monthly mean/median of photosynthetic impact on CO_2 fluxes and respiration-derived

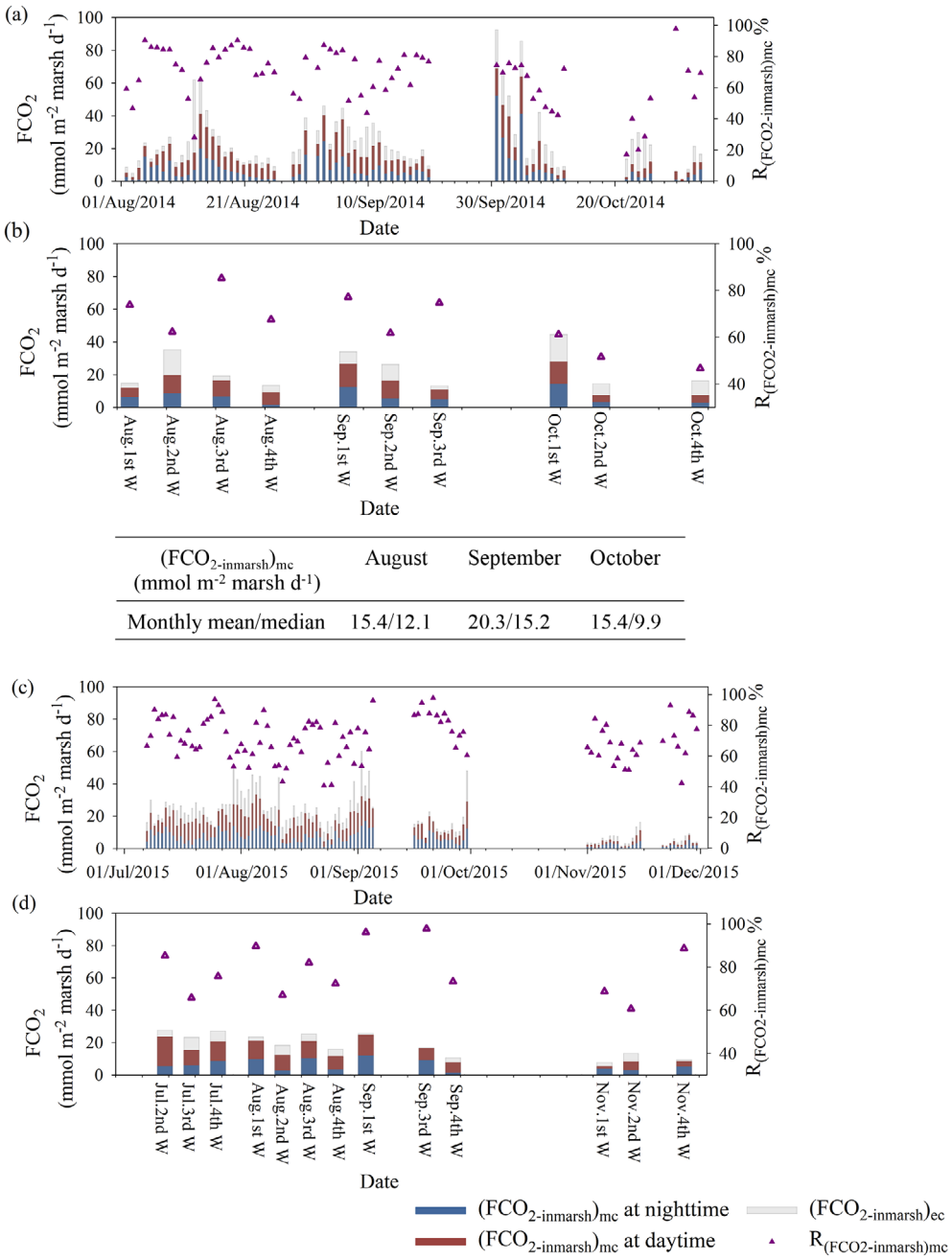

$(FCO_{2\text{-inmarsh}})_{mc}$ (mmol m^{-2} marsh d^{-1})	August	September	October
Monthly mean/median	15.4/12.1	20.3/15.2	15.4/9.9

$(FCO_{2\text{-inmarsh}})_{mc}$ (mmol m^{-2} marsh d^{-1})	July	August	September	November
Monthly mean/median	18.5/17.3	17.1/17.3	16.5/14.6	3.7/3.1

Fig. 8. Daily (**a**, **c**), and weekly (**b**, **d**) mean estuarine-contributed ($(FCO_{2\text{-inmarsh}})_{ec}$) and marsh-contributed CO_2 fluxes ($(FCO_{2\text{-inmarsh}})_{mc}$) in the inundated marsh at nighttime and daytime over the sampled periods in 2014 (**a**, **b**) and 2015 (**c**, **d**). The $R_{(FCO2inmarsh)mc}$ represents the ratio of $(FCO_{2\text{-inmarsh}})_{mc}$ to the total CO_2 efflux from the inundated marsh. The tables below each set of the figure shows the monthly means and medians of marsh-contributed CO_2 fluxes in the inundated marsh. W in the *x*-axis label in (**b**) and (**d**) means week.

CO_2 effluxes were observed in October (Fig. 9). In 2015, the absolute maximum weekly mean photosynthetic impact was observed in August. The absolute monthly median photosynthetic impact on CO_2 fluxes decreased from July to November (Fig. 9), accounting for 20–34% of the respiration-derived CO_2 effluxes from inundated marsh (Fig. 9).

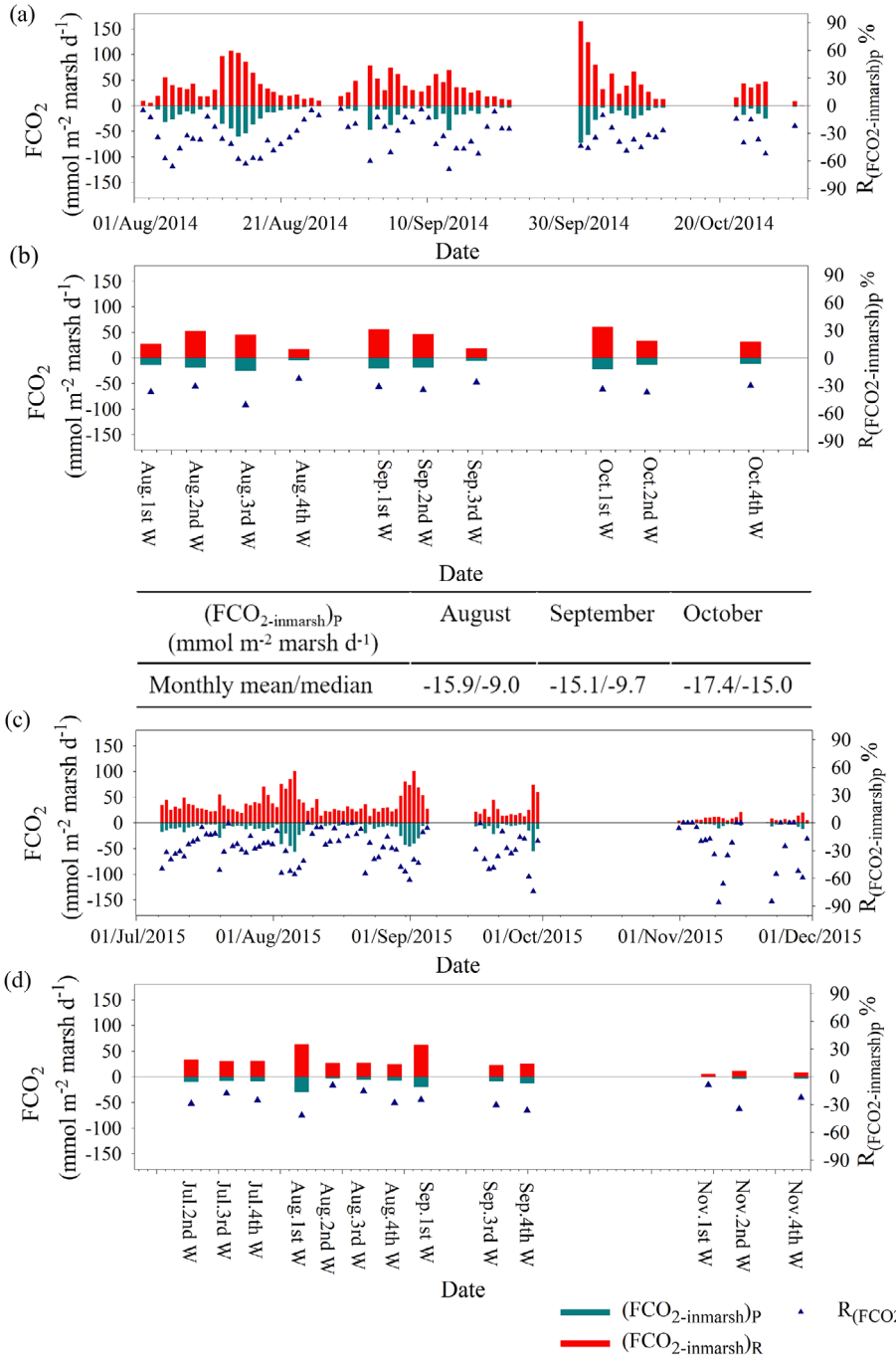

$(FCO_{2\text{-inmarsh}})_P$ (mmol m^{-2} marsh d^{-1})	August	September	October
Monthly mean/median	-15.9/-9.0	-15.1/-9.7	-17.4/-15.0

$(FCO_{2\text{-inmarsh}})_P$ (mmol m^{-2} marsh d^{-1})	July	August	September	November
Monthly mean/median	-9.2/-8.6	-12.8/-6.0	-13.8/-5.7	-2.7/-1.7

Fig. 9. Daily (**a**, **c**) and weekly (**b**, **d**) mean of photosynthetic impact on CO_2 fluxes ($(FCO_{2\text{-inmarsh}})_P$) and the ratio of the daily photosynthetic impact on CO_2 flux to the daily respiration-derived CO_2 efflux ($(FCO_{2\text{-inmarsh}})_R$) in the inundated marsh ($R_{(FCO2\text{-inmarsh})P}$) in 2014 (**a**, **b**) and 2015 (**c**, **d**). The tables below each set of the figure shows the monthly means and medians of the impact of photosynthesis on CO_2 fluxes in the inundated marsh. W in the *x*-axis label in (**b**) and (**d**) means week. The negative value indicated that photosynthesis impacts are to reduce CO_2 fluxes to the atmosphere.

Discussion

The importance of high-frequency measurements in CO_2 flux estimation

Vertical CO_2 evasion of marsh carbon through the air–water interface in the inundated marsh, including the intermittently flooded platform and the tidal creek, likely played an important role in the salt marsh carbon cycle (Figs. 6, 7). However, less attention has been directed to air–water CO_2 evasion in both the tidal creek and flooded marsh platform in past studies (Trifunovic et al. 2020). Wang and Cai (2004) reported an estimate of total air–water CO_2 efflux of ~ 56 g C m^{-2} marsh yr^{-1} over the inundated salt marsh including the tidal creek and flooded marsh platform in the Duplin River based on two discrete samplings at high and low tides over a given tidal cycle across seasons. The low frequency of sampling likely led to large uncertainties in estimated air–water CO_2 efflux from the inundated marsh.

This study estimated CO_2 effluxes from the inundated marsh based on high-frequency measurements of pCO_2 enhanced by data gap-filling using deep learning algorithms. We conducted a frequency analysis of inundated marsh CO_2 effluxes in August and October 2014 (Supporting Information Fig. S3) and found that inundated marsh CO_2 effluxes do not follow a normal distribution for both months. It is likely that lower frequency sampling of tidal CO_2 fluxes from salt marshes (e.g., over a few tidal cycles) would fail to capture the true flux and result in large errors in estimating CO_2 fluxes over longer time scales (e.g., monthly, seasonally, and annually). Therefore, it is of great importance to measure or accurately model high-frequency variability in air–water CO_2 flux over all temporal scales of interest.

Marsh carbon as a dominant term in CO_2 evasion

In this study, marsh-contributed CO_2 flux in the inundated marsh accounted for 17–98% (mean = 69%) of the total CO_2 evasion in the inundated marsh (Fig. 8), indicating that the salt marsh-sourced carbon fueled a majority of the CO_2 evasion of marsh-influenced tidal water. Previous studies have reported that the mangrove creek CO_2 fluxes were mostly controlled by the exchange with sediment porewater, even though in situ processes (e.g., photosynthesis and respiration) may also affect CO_2 fluxes (Koné and Borges 2008; Call et al. 2015; Sippo et al. 2017). Marsh sediment porewater DIC export likely accounts for the majority of the marsh-contributed CO_2 fluxes, compared to respiration of organic carbon in the tidal water. According to Zhu et al. (2022), the marsh porewater-derived carbon accounted for $\sim 75\%$ of the total air–water CO_2 evasion in a salt marsh of Hangzhou Bay, China. Tamborski et al. (2021) reported significant porewater exchange in the upper 5 cm of the marsh surface (0–36 L m^{-2} d^{-1}) in our study site, which translated to 145–521 mmol m^{-2} d^{-1} DIC ($\sim$ 57–203 mmol m^{-2} d^{-1} [CO_2*]) export in summer and fall. This exported DIC is likely sufficient to support CO_2 fluxes reported in this study (1–67 mmol m^{-2} marsh d^{-1}; Figs. 6, 7). The CO_2 fluxes at low tides were on average ~ 20 times of those at high tides for the study periods (Supporting Information Fig. S4), which provides additional evidence of the significant contribution of marsh porewater to CO_2 evasion in tidal water. Moreover, to the extent that respiration in the tidal creek contributed to CO_2 fluxes, the substrate organic carbon is mostly produced from marsh production (Santos et al. 2009, 2019). Therefore, the marsh-contributed CO_2 flux in the inundated marsh is mostly supported by marsh sediment porewater exports and likely to a lesser degree by water-column respiration of organic carbon with marsh origin.

The marsh-contributed CO_2 fluxes in summer were greater than in late autumn (Fig. 8), likely due to a higher respiration rate in summer as a result of the well-known sensitivity of ecosystem respiration to temperature (Lloyd and Taylor 1994; Mahecha et al. 2010; Tong et al. 2014). A large difference was observed between the nighttime and daytime marsh-contributed CO_2 flux, likely resulting from photosynthetic influence as well as differences in wind speed and temperature between nighttime and daytime. These results highlight the necessity to measure both nighttime and daytime conditions to accurately estimate the total flux.

There are likely two factors affecting the uncertainties of marsh-contributed CO_2 flux. First, we assumed pCO_2 values in the flooded platform were equal to that at the mouth of tidal creek. This could underestimate the contribution of the marsh to tidal water CO_2 evasion, given that the marsh continuously contributes CO_2 to the tidal water through porewater exchange and through water-column respiration after the tidal water flows onto the marsh platform. Therefore, our estimation of marsh-contributed CO_2 flux likely represents a conservative value. Second, we assumed the dissolved CO_2 concentration, [CO_2*], in the estuarine endmember was constant over each day, which could introduce uncertainties in the marsh-contributed CO_2 flux estimate, as respiration/photosynthesis can change DIC, thus [CO_2*], in the estuarine water endmember. However, [CO_2*] in estuarine water is lower than the tidal water exchanged with the marsh most of the time, and its variation is likely minimal (mean pCO_2 value at the high tide was 786 μatm with a range of 237–1440 μatm in August) compared to pCO_2 in low tide water (mean 4678 μatm, with a range of 292–8924 μatm in August; Fig. 3). As such, the uncertainties due to the assumption of constant dissolved CO_2 concentrations in estuarine endmember over each daytime–nighttime period should be limited.

Photosynthesis in tidal water as a significant factor reducing CO_2 evasion

Our analysis suggests that photosynthesis in the inundated marsh reduced CO_2 flux by a large proportion (1–86%, mean $\sim 31\%$) of daily respiration-derived CO_2 efflux during the sampling periods, indicating a high photosynthetic rate in tidal

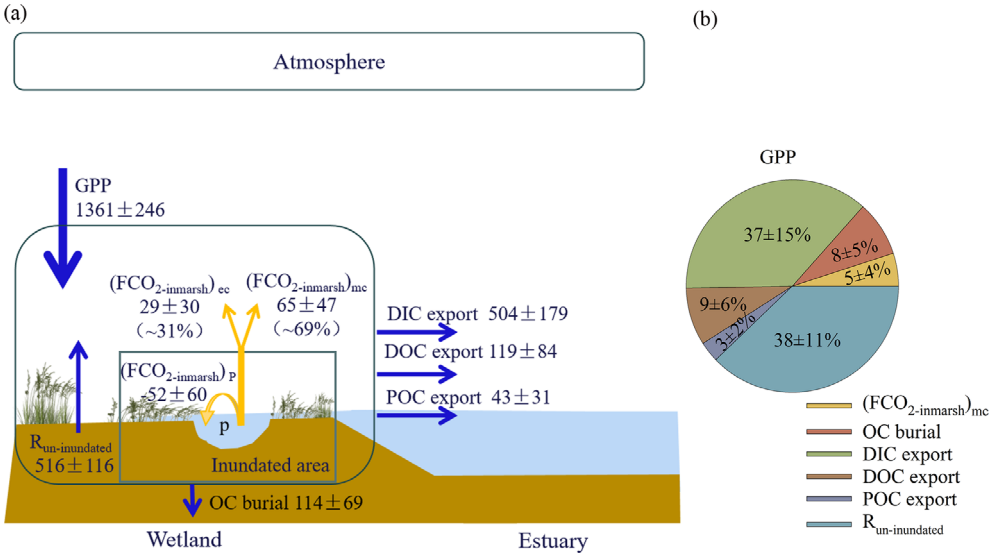

Fig. 10. The major salt marsh carbon fluxes (**a**) and their percentages of marsh gross primary production (GPP) (**b**) over the summer and fall in the U.S. Northeast Coast (including the Mid-Atlantic Bight and Gulf of Maine). The flux numbers in (**a**) represent mean marsh areal fluxes over summer and fall (g C m^{-2} marsh yr^{-1}) with corresponding one standard deviation. The lateral POC and DOC exports were mean values of summer and fall reported in Herrmann et al. (2015) and Najjar et al. (2018); the lateral DIC export is from Wang et al. (2016); the respiration in un-inundated marsh is from Forbrich and Giblin (2015) and Carey et al. (2022); carbon burial is the annual mean value from Chmura et al. (2003). GPP = $(FCO_{2\_inmarsh})_{mc}$ + OC burial + DIC export + DOC export + POC export + $R_{un\text{-}inundated}$ in the figure. The numbers indicated by yellow arrows are from this study. P denotes photosynthesis in tidal water; $R_{un\text{-}inundated}$ denotes respiration in un-inundated marsh. Also shown are the photosynthetic impact on CO_2 flux ($(FCO_{2\_inmarsh})_p$), marsh-contributed CO_2 flux ($(FCO_{2\_inmarsh})_{mc}$), and estuarine-contributed CO_2 flux ($(FCO_{2\_inmarsh})_{ec}$) from the inundated marsh, including the tidal creek and flooded marsh platform.

water throughout summer and autumn (Fig. 9). The magnitude of monthly mean CO_2 fluxes reduced by photosynthesis in the inundated marsh was higher than the corresponding marsh-contributed CO_2 fluxes in October 2014, and slightly lower in the other studied months of 2014 and 2015 (Figs. 8, 9). This suggests photosynthesis in tidal water can exert a major influence on marsh carbon evasion.

Three types of primary producers including phytoplankton, algae, and marsh grass might contribute to the primary production in tidal creeks of salt marshes (Stribling and Cornwell 1997). Previous studies have reported that phytoplankton and algae contributed an important portion of primary production in tidal creeks of salt marshes (Haines 1977; Sherr 1982; Peterson and Howarth 1987). Given the photosynthesis-reduced CO_2 flux in the inundated marsh, some portion of marsh-released DIC might be converted to organic carbon by phytoplankton/algae photosynthesis. As a comparison, the monthly mean photosynthesis-reduced CO_2 fluxes are equivalent to 6–10% and 2–26% of the lateral DIC fluxes estimated at SLP in summer and fall (Wang et al. 2016), respectively. Some of the fixed carbon might be laterally exported to the estuary and coastal ocean through tidal exchange as particulate organic carbon (POC) or DOC. As such, a portion of the lateral export of DOC and POC from the marsh might be originally from marsh-released DIC. Future studies are needed to further parse the complex interaction between different carbon pools during the lateral export processes to better assess the magnitude and fate of these lateral fluxes.

The role of tidal water CO_2 fluxes

The lateral DIC fluxes exported from this marsh during a similar period (2012–2014) have been reported by Wang et al. (2016), as the time-integrated net exchange between the SLP marsh and Waquoit Bay, measured at the same time-series location (i.e., the mouth of the SLP tidal creek; Fig. 1). Based on the lateral DIC flux reported by Wang et al. (2016), the net CO_2 evasion of marsh-sourced carbon estimated in this study equals 3–23% (mean ~ 13%) of the corresponding monthly marsh lateral DIC fluxes. As such, the vertical CO_2 evasion in the inundated marsh was an important loss term for the marsh carbon budget. Moreover, we found that the high rates of photosynthesis in tidal water significantly reduced air–water CO_2 fluxes during the sampling periods in 2014 and 2015. This decrease equals 2–26% (mean ~ 11%) of the marsh lateral DIC fluxes during the same sampling period.

To gain more insight on the role of the CO_2 fluxes in the inundated marsh, we converted the various CO_2 flux terms estimated in this study to annualized mean values of summer and fall in order to compare them with other mean carbon fluxes of the same seasons from the salt marshes in the U.S. northeast coast including the Mid-Atlantic Bight and Gulf of Maine (Najjar et al. 2018) (Fig. 10). CO_2 flux rates were presented as annualized rates simply for the convenience of

comparison with previous reports. In Fig. 10, the mean lateral DIC, DOC, and POC fluxes and CO_2 evasion from respiration in un-inundated marsh over summer and fall were adopted from the values published in previous studies (e.g., Herrmann et al. 2015; Wang et al. 2016; Najjar et al. 2018). The annual mean carbon burial rate was from Chmura et al. (2003). The CH_4 flux was ignored in the salt marsh carbon budget, given its small contribution in the environments with relatively high salinity ($S > 15$) and high sulfate reduction rate (Moseman-Valtierra et al. 2016; Carey et al. 2022). The carbon flux comparison in Fig. 10 is not to provide definitive regional flux estimates, but rather offers comparative insight into the coastal salt marsh carbon budget.

Evasion from the tidal creek and flooded marsh platform is $\sim 94 \pm 77$ g C m^{-2} marsh yr^{-1} in summer and fall, with $\sim 69\%$ derived from the marsh and the remaining 31% has an estuarine source (Fig. 10). This evasion rate is similar to the mean salt marsh organic carbon burial rate (114 ± 69 g C m^{-2} marsh yr^{-1}), as well as the mean lateral DOC export (119 ± 84 g C m^{-2} marsh yr^{-1}) along the northeast coast (Fig. 10). In total, U.S. northeast coast salt marshes lose $\sim 569 \pm 226$ g C m^{-2} marsh yr^{-1} of inorganic carbon after exchanging with tidal water, including $\sim 11\%$ as CO_2 evasion from tidal water surface to the atmosphere in inundated marsh and $\sim 89\%$ as lateral DIC flux to adjacent estuarine and coastal waters (Fig. 10). The marsh CO_2 evasion rate from inundated areas accounted for $\sim 5 \pm 4\%$ of the marsh gross primary production (Fig. 10b). This efflux would be about 80% greater if not for preemptive photosynthetic uptake of CO_2 in tidal water ($\sim 52 \pm 60$ g C m^{-2} marsh yr^{-1}; Fig. 10).

This study presents a first attempt to quantify CO_2 evasion in the inundated area of a tidal marsh with high-resolution measurements, as well as the first to differentiate marsh-sourced vs. estuarine-sourced carbon loss in these CO_2 fluxes. This study determined the majority of CO_2 evasion in tidal water on average is fueled by marsh carbon through respiration in marsh soil, porewater, and exchanged tidal water in summer and fall. The marsh carbon loss as CO_2 through the air–water interface in the inundated marsh is an important loss term for the marsh carbon budget. The role of photosynthetic uptake of DIC by phytoplankton/algae in tidal water is to convert an amount of DIC to organic carbon that is stored in the marsh as POC and/or exported laterally as POC and DOC. These conclusions were made based on high-frequency time-series measurements, representing a concrete step forward in resolving the complex dynamics of the CO_2 fluxes in tidal water exchanged with a salt marsh system.

Data availability statement

The data that support the findings of this study will be released by U.S. Geological Survey (https://doi.org/10.5066/P9STIROQ).

References

Abdul-Aziz, O. I., K. S. Ishtiaq, J. Tang, S. Moseman-Valtierra, K. D. Kroeger, M. E. Gonneea, J. Mora, and K. Morkeski. 2018. Environmental controls, emergent scaling, and predictions of greenhouse gas (GHG) fluxes in coastal salt marshes. J. Geophys. Res.: Biogeosciences **123**: 2234–2256. doi:10.1029/2018JG004556

Amaral, J. H. F., A. L. Suhett, S. Melo, and V. F. Farjalla. 2013. Seasonal variation and interaction of photodegradation and microbial metabolism of DOC in black water Amazonian ecosystems. Aquat. Microb. Ecol. **70**: 157–168. doi:10.3354/ame01651

Atkins, M. L., I. R. Santos, S. Ruiz-Halpern, and D. T. Maher. 2013. Carbon dioxide dynamics driven by groundwater discharge in a coastal floodplain creek. J. Hydrol. **493**: 30–42. doi:10.1016/j.jhydrol.2013.04.008

Baldocchi, D. 2014. Measuring fluxes of trace gases and energy between ecosystems and the atmosphere—the state and future of the eddy covariance method. Glob. Change Biol. **20**: 3600–3609. doi:10.1111/gcb.12649

Borges, A. V., J. P. Vanderborght, L. S. Schiettecatte, F. Gazeau, S. Ferrón-Smith, B. Delille, and M. Frankignoulle. 2004. Variability of the gas transfer velocity of CO_2 in a macrotidal estuary (the Scheldt). Estuaries **27**: 593–603. doi:10.1007/BF02907647

Cai, W. J. 2011. Estuarine and coastal ocean carbon paradox: CO_2 sinks or sites of terrestrial carbon incineration? Ann. Rev. Mar. Sci. **3**: 123–145. doi:10.1146/annurev-marine-120709-142723

Cai, W. J., and Y. Wang. 1998. The chemistry, fluxes, and sources of carbon dioxide in the estuarine waters of the Satilla and Altamaha Rivers, Georgia. Limnol. Oceanogr. **43**: 657–668. doi:10.4319/lo.1998.43.4.0657

Cai, W. J., Z. A. Wang, and Y. Wang. 2003. The role of marsh-dominated heterotrophic continental margins in transport of CO_2 between the atmosphere, the land-sea interface and the ocean. Geophys. Res. Lett. **30**: 1849. doi:10.1029/2003GL017633

Call, M., and others. 2015. Spatial and temporal variability of carbon dioxide and methane fluxes over semi-diurnal and spring-neap-spring timescales in a mangrove creek. Geochim. Cosmochim. Acta **150**: 211–225. doi:10.1016/j.gca.2014.11.023

Carey, J. C., K. D. Kroeger, and J. Tang. 2022. Higher temperature sensitivity of ecosystem respiration in low marsh compared to high elevation marsh ecosystems. J. Geophys. Res.: Biogeosciences **127**: e2022JG006832. doi:10.1029/2022JG006832

Chen, X., I. R. Santos, D. Hu, L. Zhan, Y. Zhang, Z. Zhao, and L. Li. 2022. Pore-water exchange flushes blue carbon from intertidal saltmarsh sediments into the sea. Limnol. Oceanogr.: Lett. **7**: 312–320. doi:10.1002/lol2.10236

Chmura, G. L., S. C. Anisfeld, D. R. Cahoon, and J. C. Lynch. 2003. Global carbon sequestration in tidal, saline wetland

soils. Glob. Biogeochem. Cycles **17**: 1111. doi:10.1029/2002gb001917

Chmura, G. L., L. Kellman, and G. R. Guntenspergen. 2011. The greenhouse gas flux and potential global warming feedbacks of a northern macrotidal and microtidal salt marsh. Environ. Res. Lett. **6**: 044016. doi:10.1088/1748-9326/6/4/044016

Chu, S. N., Z. A. Wang, M. E. Gonneea, K. D. Kroeger, and N. K. Ganju. 2018. Deciphering the dynamics of inorganic carbon export from intertidal salt marshes using high-frequency measurements. Mar. Chem. **206**: 7–18. doi:10.1016/j.marchem.2018.08.005

Dickson, A. G. 1990. Thermodynamics of the dissociation of boric acid in potassium chloride solutions from 273.15 to 318.15 K. J. Chem. Eng. Data **35**: 253–257. doi:10.1021/je00061a009

Dickson, A. G., and J. P. Riley. 1979. The estimation of acid dissociation constants in seawater media from potentionmetric titrations with strong base. I. The ionic product of water—K_w. Mar. Chem. **7**: 89–99. doi:10.1016/0304-4203(79)90001-X

Dickson, A. G., C. L. Sabine, and J. R. Christian. 2007. Guide to best practices for ocean CO_2 measurements. North Pacific Marine Science Organization.

Douglas, N. K., and R. H. Byrne. 2017. Spectrophotometric pH measurements from river to sea: Calibration of mCP for $0 \leq S \leq 40$ and $278.15 \leq T \leq 308.15$ K. Mar. Chem. **197**: 64–69. doi:10.1016/j.marchem.2017.10.001

Duarte, C. M., J. J. Middelburg, and N. Caraco. 2005. Major role of marine vegetation on the oceanic carbon cycle. Biogeosciences **2**: 1–8. doi:10.5194/bg-2-1-2005

Dušek, J., H. Čížková, R. Czerný, K. Taufarová, M. Šmídová, and D. Janouš. 2009. Influence of summer flood on the net ecosystem exchange of CO_2 in a temperate sedge-grass marsh. Agric. For. Meteorol. **149**: 1524–1530. doi:10.1016/j.agrformet.2009.04.007

Forbrich, I., and A. E. Giblin. 2015. Marsh-atmosphere CO_2 exchange in a New England salt marsh. J. Geophys. Res.: Biogeosciences **120**: 1825–1838. doi:10.1002/2015JG003044

Gonneea, M. E., and others. 2019. Salt marsh ecosystem restructuring enhances elevation resilience and carbon storage during accelerating relative sea-level rise. Estuar. Coast. Shelf Sci. **217**: 56–68. doi:10.1016/j.ecss.2018.11.003

Haines, E. B. 1977. The origins of detritus in Georgia salt marsh estuaries. Oikos **29**: 254. doi:10.2307/3543611

Herrmann, M., and others. 2015. Net ecosystem production and organic carbon balance of US East Coast estuaries: A synthesis approach. Glob. Biogeochem. Cycles **29**: 96–111. doi:10.1002/2013GB004736

Ho, D. T., V. C. Engel, S. Ferrón, B. Hickman, J. Choi, and J. W. Harvey. 2018. On factors influencing air-water gas exchange in emergent wetlands. J. Geophys. Res.: Biogeosciences **123**: 178–192. doi:10.1002/2017JG004299

Hopkinson, C. S., W. J. Cai, and X. Hu. 2012. Carbon sequestration in wetland dominated coastal systems—a global sink of rapidly diminishing magnitude. Curr. Opin. Environ. Sustain. **4**: 186–194. doi:10.1016/j.cosust.2012.03.005

Koeve, W., and A. Oschlies. 2012. Potential impact of DOM accumulation on fCO_2 and carbonate ion computations in ocean acidification experiments. Biogeosciences **9**: 3787–3798. doi:10.5194/bg-9-3787-2012

Koné, Y. J. M., and A. V. Borges. 2008. Dissolved inorganic carbon dynamics in the waters surrounding forested mangroves of the Ca Mau Province (Vietnam). Estuar. Coast. Shelf Sci. **77**: 409–421. doi:10.1016/j.ecss.2007.10.001

Kuehn, K. A., D. Steiner, and M. O. Gessner. 2004. Diel mineralization patterns of standing-dead plant litter: Implications for CO_2 flux from wetlands. Ecology **85**: 2504–2518. doi:10.1890/03-4082

Landschützer, P., N. Gruber, D. C. E. Bakker, and U. Schuster. 2014. Recent variability of the global ocean carbon sink. Glob. Biogeochem. Cycles **28**: 927–949. doi:10.1002/2014GB004853

Large, W. G., and S. Pond. 1981. Open ocean momentum flux measurements in moderate to strong winds. J. Phys. Oceanogr. **11**: 324–336. doi:10.1175/1520-0485(1981)011<0324:OOMFMI>2.0.CO;2

Lloyd, J., and J. A. Taylor. 1994. On the temperature dependence of soil respiration. Funct. Ecol. **8**: 315–323. doi:10.2307/2389824

Lohrenz, S. E., W. Cai, F. Chen, X. Chen, and M. Tuel. 2010. Seasonal variability in air-sea fluxes of CO_2 in a river-influenced coastal margin. J. Geophys. Res.: Oceans **115**: C10034. doi:10.1029/2009JC005608

Mahecha, M. D., and others. 2010. Global convergence in the temperature sensitivity of respiration at ecosystem level. Science **329**: 838–840. doi:10.1126/science.1189587

McLeod, E., and others. 2011. A blueprint for blue carbon: Toward an improved understanding of the role of vegetated coastal habitats in sequestering CO_2. Front. Ecol. Environ. **9**: 552–560. doi:10.1890/110004

Moseman-Valtierra, S., and others. 2016. Carbon dioxide fluxes reflect plant zonation and belowground biomass in a coastal marsh. Ecosphere **7**: e01560. doi:10.1002/ecs2.1560

Najjar, R. G., and others. 2018. Carbon budget of tidal wetlands, estuaries, and shelf waters of eastern North America. Glob. Biogeochem. Cycles **32**: 389–416. doi:10.1002/2017GB005790

Nezlin, N. P., K. Kamer, J. Hyde, and E. D. Stein. 2009. Dissolved oxygen dynamics in a eutrophic estuary, Upper Newport Bay, California. Estuar. Coast. Shelf Sci. **82**: 139–151. doi:10.1016/j.ecss.2009.01.004

Osburn, C. L., M. P. Mikan, J. R. Etheridge, M. R. Burchell, and F. Birgand. 2015. Seasonal variation in the quality of dissolved and particulate organic matter exchanged between a salt marsh and its adjacent estuary. J. Geophys. Res.: Biogeosciences **120**: 1430–1449. doi:10.1002/2014JG002897

Peterson, B. J., and R. W. Howarth. 1987. Sulfur, carbon, and nitrogen isotopes used to trace organic matter flow in the salt-marsh estuaries of Sapelo Island, Georgia. Limnol. Oceanogr. **32**: 1195–1213. doi:10.4319/lo.1987.32.6.1195

Raven, J. A., C. J. Gobler, and P. J. Hansen. 2020. Dynamic CO_2 and pH levels in coastal, estuarine, and inland waters: Theoretical and observed effects on harmful algal blooms. Harmful Algae **91**: 101594. doi:10.1016/j.hal.2019.03.012

Raymond, P. A., and J. J. Cole. 2001. Gas exchange in rivers and estuaries: Choosing a gas transfer velocity. Estuaries **24**: 312–317. doi:10.2307/1352954

Rödenbeck, C., R. F. Keeling, D. C. E. Bakker, N. Metzl, A. Olsen, C. Sabine, and M. Heimann. 2013. Global surface-ocean pCO_2 and sea-air CO_2 flux variability from an observation-driven ocean mixed-layer scheme. Ocean Sci. **9**: 193–216. doi:10.5194/os-9-193-2013

Sanders-DeMott, R., and others. 2022. Impoundment increases methane emissions in *Phragmites*-invaded coastal wetlands. Glob. Change Biol. **28**: 4539–4557. doi:10.1111/gcb.16217

Santos, I. R., W. C. Burnett, T. Dittmar, I. G. Suryaputra, and J. Chanton. 2009. Tidal pumping drives nutrient and dissolved organic matter dynamics in a Gulf of Mexico subterranean estuary. Geochim. Cosmochim. Acta **73**: 1325–1339. doi:10.1016/j.gca.2008.11.029

Santos, I. R., D. T. Maher, R. Larkin, J. R. Webb, and C. J. Sanders. 2019. Carbon outwelling and outgassing vs. burial in an estuarine tidal creek surrounded by mangrove and saltmarsh wetlands. Limnol. Oceanogr. **64**: 996–1013. doi:10.1002/lno.11090

Shahan, J., and others. 2022. Combining eddy covariance and chamber methods to better constrain CO_2 and CH_4 fluxes across a heterogeneous restored tidal wetland. J. Geophys. Res.: Biogeosciences **127**: e2022JG007112. doi:10.1029/2022JG007112

Sharp, J. D., D. Pierrot, M. P. Humphreys, J.-M. Epitalon, J. C. Orr, E. R. Lewis, and D. W. R. Wallace. 2020. CO2SYSv3 for MATLAB. Zenodo.

Sherr, E. B. 1982. Carbon isotope composition of organic seston and sediments in a Georgia salt marsh estuary. Geochim. Cosmochim. Acta **46**: 1227–1232. doi:10.1016/0016-7037(82)90007-2

Sippo, J. Z., D. T. Maher, D. R. Tait, S. Ruiz-Halpern, C. J. Sanders, and I. R. Santos. 2017. Mangrove outwelling is a significant source of oceanic exchangeable organic carbon. Limnol. Oceanogr.: Lett. **2**: 1–8. doi:10.1002/lol2.10031

Song, S., Z. A. Wang, M. E. Gonneea, K. D. Kroeger, S. N. Chu, D. Li, and H. Liang. 2020. An important biogeochemical link between organic and inorganic carbon cycling: Effects of organic alkalinity on carbonate chemistry in coastal waters influenced by intertidal salt marshes. Geochim. Cosmochim. Acta **275**: 123–139. doi:10.1016/j.gca.2020.02.013

Stribling, J. M., and J. C. Cornwell. 1997. Identification of important primary producers in a Chesapeake Bay tidal creek system using stable isotopes of carbon and sulfur. Estuaries **20**: 77–85. doi:10.2307/1352721

Tamborski, J. J., M. Eagle, B. L. Kurylyk, K. D. Kroeger, Z. A. Wang, P. Henderson, and M. A. Charette. 2021. Pore water exchange-driven inorganic carbon export from intertidal salt marshes. Limnol. Oceanogr. **6**: 1774–1792. doi:10.1002/lno.11721

Tong, C., C. Wang, J. F. Huang, W. Q. Wang, E. Yan, J. Liao, and C. Yao. 2014. Ecosystem respiration does not differ before and after tidal inundation in brackish marshes of the Min River estuary, southeast China. Wetlands **34**: 225–233. doi:10.1007/s13157-013-0478-x

Trifunovic, B., A. Vázquez-Lule, M. Capooci, A. L. Seyfferth, C. Moffat, and R. Vargas. 2020. Carbon dioxide and methane emissions from a temperate salt marsh tidal creek. J. Geophys. Res.: Biogeosciences **125**: e2019JG005558. doi:10.1029/2019JG005558

Vachon, D., J. F. Lapierre, and P. A. del Giorgio. 2016. Seasonality of photochemical dissolved organic carbon mineralization and its relative contribution to pelagic CO_2 production in northern lakes. J. Geophys. Res.: Biogeosciences **121**: 864–878. doi:10.1002/2015JG003244

van Dam, B. R., J. B. Edson, and C. Tobias. 2019. Parameterizing air-water gas exchange in the shallow, microtidal New River estuary. J. Geophys. Res.: Biogeosciences **124**: 2351–2363. doi:10.1029/2018JG004908

Wang, Z. A., and W. J. Cai. 2004. Carbon dioxide degassing and inorganic carbon export from a marsh-dominated estuary (the Duplin River): A marsh CO_2 pump. Limnol. Oceanogr. **49**: 341–354. doi:10.4319/lo.2004.49.2.0341

Wang, Z. A., K. D. Kroeger, N. K. Ganju, M. E. Gonneea, and S. N. Chu. 2016. Intertidal salt marshes as an important source of inorganic carbon to the coastal ocean. Limnol. Oceanogr. **61**: 1916–1931. doi:10.1002/lno.10347

Warner, J. C., B. Armstrong, R. Y. He, and J. B. Zambon. 2010. Development of a coupled ocean–atmosphere–wave–sediment transport (COAWST) modeling system. Ocean Model. **35**: 230–244. doi:10.1016/j.ocemod.2010.07.010

Weiss, R. F. 1974. Carbon dioxide in water and seawater: The solubility of a nonideal gas. Mar. Chem. **2**: 203–215. doi:10.1016/0304-4203(74)90015-2

Zhu, P., and others. 2022. Porewater-derived blue carbon outwelling and greenhouse gas emissions in a subtropical multi-species saltmarsh. Front. Mar. Sci. **9**: 884951. doi:10.3389/fmars.2022.884951

Acknowledgment

We thank Neil Kamal Ganju, Zaiyang Zhou, Sydney K. Nick, Adrian C. Mann, Kate Morkeski for the assistance of data analysis and language improvement. This study was supported by the USGS Coastal and Marine Hazards and Resources Program, the USGS Land Change Science Program's Land Carbon program, the U.S. National Science Foundation (OCE-1459521), the NOAA Science Collaborative program (NA09NOS4190153), National Natural Science Foundation of China (41776104), and Postdoctoral Research Foundation of China (2020M681229). Any use of trade, firm or product names is for descriptive purposes only and does not imply endorsement by the U.S. Government.

Conflict of Interest

None declared.

Submitted 05 August 2022
Revised 04 July 2023
Accepted 06 July 2023

Associate editor: Vanessa Hatje